HHS Public Access

Author manuscript

Brain Stimul. Author manuscript; available in PMC 2022 April 10.

Published in final edited form as:

Brain Stimul. 2021 ; 14(4): 790–800. doi:10.1016/j.brs.2021.04.021.

Sonothermogenetics for Noninvasive and Cell-type Specific Deep Brain Neuromodulation

Yaoheng Yang[1], **Christopher Pham Pacia**[1], **Dezhuang Ye**[2], **Lifei Zhu**[1], **Hongchae Baek**[1], **Yimei Yue**[1], **Jinyun Yuan**[1], **Mark J. Miller**[3], **Jianmin Cui**[1], **Joseph P. Culver**[1,4,5], **Michael R. Bruchas**[6], **Hong Chen**[1,7,*]

[1.]Department of Biomedical Engineering, Washington University in St. Louis, Saint Louis, MO 63130, USA.

[2.]Department of Mechanical Engineering and Materials Science, Washington University in St. Louis, Saint Louis, MO 63130, USA

[3.]Division of Infectious Diseases, Department of Medicine, Washington University School of Medicine, Saint Louis, MO, USA

[4.]Mallinckrodt Institute of Radiology, Washington University School of Medicine, Saint Louis, MO 63110, USA.

[5.]Department of Physics, Washington University in St. Louis, Saint Louis, MO 63110, USA

[6.]Department of Anesthesiology and Pain Medicine. Center for Neurobiology of Addiction, Pain, and Emotion. University of Washington, Seattle, WA 98195, USA

[7.]Department of Radiation Oncology, Washington University School of Medicine, Saint Louis, MO 63108, USA.

Abstract

Background: Critical advances in the investigation of brain functions and treatment of brain disorders are hindered by our inability to selectively target neurons in a noninvasive manner in the deep brain.

Objective: This study aimed to develop sonothermogenetics for noninvasive, deep-penetrating, and cell-type-specific neuromodulation by combining a thermosensitive ion channel TRPV1 with focused ultrasound (FUS)-induced brief, non-noxious thermal effect.

[*]Address correspondence to Hong Chen, Ph.D. Department of Biomedical Engineering and Radiation Oncology, Washington University in St. Louis. 4511 Forest Park Ave. St. Louis, MO, 63108, USA. hongchen@wustl.edu.

Author contributions

H.C. formulated the overarching research goals and aims. H. C. and Y. Y. designed the experiments. Y. Y. conducted the experiment with the assistant of other co-authors. J.Y. assisted with the *in vitro* experiment. D.Y and M.M assisted with setting up the two-photon microscopy system. L.Z and C.P assisted with the MR thermometry experiment. H.B and Y.Y assisted with animal surgery. Y.Y performed the immunohistochemistry staining experiment. J.C, J. P.C, and M. R.B contributed to the discussion and interpretation of the results. H.C and Y.Y wrote the manuscript, and all authors modified and revised the manuscript.

Declaration of Interests

The authors have declared that no competing interest exists.

Data statement

The data that support the findings of this study are available from the corresponding author upon reasonable request.

Methods: The sensitivity of TRPV1 to FUS sonication was evaluated *in vitro*. It was followed by *in vivo* assessment of the success rate of sonothermogenetics in the activation of genetically defined neurons in the mouse brain by two-photon microscopic calcium imaging. Behavioral response evoked by sonothermogenetic stimulation at a deep brain target was recorded in freely moving mice. Immunohistochemistry staining of *ex vivo* brain slices was performed to evaluate the safety of FUS sonication.

Results: TRPV1 was found to be an ultrasound-sensitive ion channel. FUS sonication at the mouse brain *in vivo* selectively activated neurons that were genetically modified to express TRPV1. Temporally precise activation of TRPV1-expressing neurons was achieved with its success rate linearly correlated with the peak temperature within the FUS-targeted brain region as measured by *in vivo* magnetic resonance thermometry. FUS stimulation of TRPV1-expressing neurons at the striatum repeatedly evoked locomotor behavior in freely moving mice. FUS sonication was confirmed to be safe based on inspection of neuronal integrity, inflammation, and apoptosis markers.

Conclusions: This noninvasive and cell-type-specific neuromodulation approach with the capability to target the deep brain has the promise to advance the study of the intact nervous system and uncover new ways to treat neurological disorders.

Keywords

Sonothermogenetics; Ion channel; Focused ultrasound; Neuromodulation; Calcium imaging

Introduction

Critical advances in the investigation of brain functions and treatment of brain disorders require noninvasive neuromodulation techniques for causal control of specific neuron types without the need for surgical implantation of any devices. Deep brain stimulation has become a treatment option for some neurological disorders such as Parkinson's disease and epilepsy [1,2], but requires surgical implantation of electrodes and lacks cell-type specificity. Existing noninvasive approaches, such as electrical, magnetic, and ultrasound neuromodulation, unselectively stimulate different types of neurons and nonneuronal cells within the targeted region, resulting in neuromodulation with relatively low reliability and replicability [3,4]. Advances in genetics-based tools enable manipulation of a specific type of neuron embedded within densely wired brain circuits for assessing the causal role that different groups of neurons play in controlling circuit activity and behavior outcomes. Among existing genetics-based tools, optogenetics has boosted the discovery of new neural circuitries, the activation or inhibition of which can rescue neurological deficits in mice [5]. However, optogenetics often requires surgery for the permanent implantation of optical fibers to the brain to deliver light. Surgical implantation damages tissue and increases infection and ischemia risk, which constitute the major barrier for fulfilling the promise of optogenetics for the treatment of neurological disorders in the clinic. It was recently reported that noninvasive deep brain optogenetics is feasible with red-shifted opsins that can be activated by transcranial red light illumination [6,7]. Although transcranial red light can penetrate deep into the mouse brain, it loses the capability to target selected brain regions due to the diffusion of light.

Focused ultrasound (FUS) has the potential to noninvasively target any area in the whole brain in animal models and humans [8-10]. Its combined depth penetration and spatial focusing cannot be achieved by other external stimulation modalities (e.g., optical, electrical, and magnetic stimulation). Although ultrasound is well known to be associated with both mechanical and thermal effects, the current paradigm in FUS neuromodulation utilizes the ultrasound mechanical effect by using pulsed ultrasound with a short duration (≤ 0.5 s) [11] to minimize heating (≤0.7° C) [12]. Several mechanosensitive ion channels and proteins have been proposed as sonogenetic actuators, for example TREK-1/2 [13], MscL [14], Piezo1 [15], TRPA1 [16], Mscl-G22S [17], and prestin [18]. However, most reported studies were performed *in vitro* with only preliminary *in vivo* studies suggesting that some of these channels can be activated by ultrasound in the mouse brain [19]. Recent technological advances have enabled noninvasive and spatially targeted FUS heating in the human brain with precise control of temperature based on real-time temperature monitoring using magnetic resonance (MR) thermometry [20]. The United States Food and Drug Administration (FDA) approved FUS thermal therapy for the treatment of medication-refractory essential tremor in 2016. Since then, ablative high-intensity FUS has been investigated in the clinic for the treatment of an ever-widening set of neurological diseases, such as Parkinson's disease and chronic neuropathic pain [21,22]. FUS has also been investigated in clinical trials for hyperthermia treatment by raising tissue temperatures to 40–45 °C for up to 60 minutes, as an adjuvant to radiotherapy and chemotherapy, or for thermal-controlled drug release [23].

Here, we developed sonothermogenetics building on the technological advances in FUS thermal therapies. Sonothermogenetics uses low-intensity FUS to generate a short pulse that elevates the tissue temperature to approximately 42 °C, which activates neurons that have been genetically selected to express a thermosensitive ion channel – transient receptor potential vanilloid 1 (TRPV1). As a member of the thermosensitive transient receptor potential channel (ThermoTRP) family, TRPV1 is exquisitely sensitive to temperature. The single-channel conductance of a ThermoTRP is ~1,000-fold greater than that of an optogenetic ion channel, for example, channelrhodopsin [24]. TRPV1 has an activation temperature of approximately 42 °C [25], which is only a few degrees higher than body temperature, thus permitting quick and safe stimulation while allowing the channels to be closed at physiological temperature and minimizing other potential thermal effects on neural circuits [24,26,27]. We show that TRPV1-based sonothermogenetics enables noninvasive, cell type-specific, temporally precise control of mammalian neural activity. Deep brain stimulation is important for the therapeutic applications of neuromodulation. We provide evidence that sonothermogenetics evokes behavioral responses in freely moving mice by targeting a deep brain site (the striatum). Sonothermoegentics has the potential to transform our approaches for neuroscience research and uncover new methods to understand and treat human brain disorders.

Methods

In vitro cell culture experiment.

Our first experiment was performed to determine whether TRPV1 is a sonothermogenetic actuator by evaluating whether FUS could selectively control intracellular Ca^{2+} influx in TRPV1-expressing HEK293T cells (see Supplementary Information for more details). We developed an experimental setup that allows simultaneous fluorescence imaging and FUS stimulation of HEK293T cells (Fig. S1). The TRPV1 transgene was placed under the excitatory neuronal promoter calmodulin kinase II a-subunit and linked with mCherry by the posttranscriptional cleavage linker p2A (CaMKII-TRPV1-p2A-mCherry) [28]. This transgene was packed into a lentiviral vector and transfected to HEK293T cells *in vitro* to express TRPV1 (Fig. S2). Cells that were transfected by the control lentivirus (CaMKII-mCherry) without TRPV1 were used as control. Fluo-4 AM (Thermo Fisher Scientific), a calcium (Ca^{2+}) indicator, was used to image the dynamics of Ca^{2+} response to FUS stimulation using a fluorescence microscope (LX70, Olympus). The expression of TRPV1 in the HEK293T cells was confirmed to be mainly localized on the plasma membrane (Fig. S3a). The functionality of TRPV1 was confirmed by the observation of Ca^{2+} influx in response to capsaicin, a TRPV1 agonist (Fig. S3b). FUS (frequency = 1.7 MHz, peak negative pressure = 1.0 MPa, duty cycle = 40%, PRF = 10 Hz, duration = 30 s) was applied to the cells with and without TRPV1 expression. An additional control experiment was performed by adding TRPV1 antagonist capsazepine [40,41] before FUS stimulation. Calcium images were recorded during FUS sonication, and the local temperature rise was simultaneously recorded using a fiber-optic thermometer (Luxtron, now LumaSense Technologies). For the positive control experiment, the cells were heated by water-bath heating using the resistor-based heating unit.

In vivo two-photon calcium imaging experiment.

After establishing TRPV1 as a sonothermogenetic actuator through *in vitro* experiments, we then tested whether FUS could selectively activate $TRPV1^+$ neurons in the mouse brain *in vivo.* Lentivirus (1.0 μl of pLenti-CaMKII-TRPV1-p2A-mCherry-WPRE solution or 0.64 μl pLenti-CaMKII-mCherry-WPRE to achieve the same viral vector number) was injected into the somatosensory cortex (−0.5 mm dorsoventral, −1.2 mm anterior-posterior, and −1.2 mm mediolateral) of Thy1-GCaMP6f mice (Jackson Laboratory) following the intracranial injection procedure described in the Supplementary Information. At 4–6 weeks following virus injection, mice were used for FUS stimulation with simultaneous *in vivo* two-photon microscopic imaging (2PM) to record the neural activity based on the GCaMP6f, a Ca^{2+} indicator. Sparse expression of TRPV1 was achieved with 2 – 4 neurons co-expressing TRPV1 and GCaMP6f in the small field of view (FOV) of the 2PM images to minimize crosstalk among $TRPV1^+$ neurons once activated and allow morphological recognition of each individual $TRPV1^+$ neurons [29]. We intentionally avoided using electrophysiological recordings because electrodes inserted in the brain interfere with ultrasound wave propagation, and ultrasound wave-induced mechanical vibration generates artifacts in electrical recordings.

Before 2PM imaging, a chronic cranial window was created on the mouse head to obtain optical access to the mouse cerebral cortex for time-lapse Ca^{2+} imaging using 2PM following an established protocol [30]. After the optical window surgery, the mice were anesthetized and head-fixed for acquiring *in -vivo* time-lapse 2PM images (see Supplementary Information) with a custom-built 2PM microscope [31] during FUS stimulation.

The FUS transducer was specially designed so that the inner edge of the ring FUS transducer geometrically fit the outer edge of the microscope objective to align the optical beam and FUS beam confocally. In the repeated FUS stimulation studies, the interval between two sequential stimulations was 80 s to minimize interference among repeated stimulations. A total of 5 different parameter groups were evaluated with the ultrasound frequency (1.7 MHz) and peak negative pressure (1.3 MPa) kept the same among all the groups: (1) pulsed wave (PW) with a duty cycle of 40% and total sonication duration of 15 s; (2) PW with a duty cycle of 40% and duration of 7 s; (3) continuous wave (CW) with a duty cycle of 100% and duration of 7 s; (4) CW with a duty cycle of 100% and duration of 4 s; (5) CW with a duty cycle of 100% and duration of 1 s. For group 1, we imaged a total of 17 neurons with coexpression of TRPV1 and GCaMP6f from 6 mice injected with the lentiviral vector encoding TRPV1. Two repeated FUS stimulations were delivered to each of these neurons. For comparison purposes, we imaged 16 neurons from 5 control mice with overexpression of mCherry without TRPV1 ($TRPV1^{-}$). To test the temporal precision and repeatability of different FUS parameters, we applied 10 repeated stimuli to 5 individual neurons in mice from groups 2–5, which provided a total of 50 measurements of Ca^{2+} signals for each FUS parameter set. To minimize the activation of the auditory pathway by FUS sonication [32], we used a pulse repetition frequency of 10 Hz for groups 1 and 2, which is outside the mouse hearing range [33], and smoothed the onset and offset of each ultrasound stimulus in all groups [34].

Calcium imaging data analysis.

The calcium images recorded in the *in vitro* cell culture experiment were analyzed by MATLAB using a published algorithm [35]. Cells were automatically identified after applying a constrained nonnegative matrix factorization (CNMF) framework. Then, 100 cells were randomly selected from independent trials. Relative fluorescence intensity changes were computed for Ca^{2+} signal as $\Delta F/F=(F-F_0)/F_0$, where F_0 represents the average of a 1.5 s-long fluorescent signal acquired before FUS onset. Successful FUS stimulation was defined by the criteria that the normalized Ca^{2+} fluorescence intensity ($\Delta F/F$) acquired from the onset of FUS stimulation to 1.5-s after FUS was both >0.1 and > 2× standard deviation (SD) of 1.5 s-long signals acquired before FUS [36]. The percentage of responsive cells was calculated by dividing the number of successfully stimulated cells over the total number of all selected cells.

For the *in vivo* study, regions of interest were manually selected to cover individual soma of the neurons expressing both GCaMP6f and mCherry with TRPV1 ($TRPV1^{+}$ neurons) and without TRPV1 ($TRPV1^{-}$ neurons). Successful FUS stimulation was defined as the same as the above *in vitro* study ($\Delta F/F > 0.1$ and >2× SD). The success rate was quantified by

the proportion of successful FUS stimulations to all the applied stimulations for every single neuron. The mean success rate was then calculated by averaging the success rate over all mCherry and GCaMP6f double-positive neurons in each mouse. Latency to threshold was defined as the time from the onset of FUS to the onset of a successful stimulation. Time to 50% relaxation was defined as the time when the Ca^{2+} signal reached its peak amplitude to the time that it decayed to half of the peak amplitude.

In vivo MR thermometry.

MR thermometry was used to noninvasively image the spatiotemporal distribution of FUS-induced temperature rise in the mouse brain *in vivo*. MR thermometry is an established technique that can provide noninvasive, real-time, volumetric, and quantitative temperature measurements during FUS sonication [37,38]. BALB/c mice without viral injection were used in this study. MR thermometry was performed using a 4.7 T MRI system (Agilent/Varian DirectDrive Console). Temperature images were acquired using a continuously applied gradient-echo imaging sequence with a flip angle of 20 degrees, T_R of 10 ms and T_E of 4 ms, slice thickness of 1.5 mm, and matrix size of 128 × 128 for 60 × 60 mm FOV. Phase images were processed in real-time using ThermoGuide software (Image Guided Therapy).

An MR-compatible FUS transducer (Image Guided Therapy) was targeted at the same brain location as the 2PM study. During the experiments, mice were anesthetized using 1–2% isoflurane and placed in a small animal cradle coupled with an MRI saddle coil (Image Guided Therapy, Pessac, France). The mouse head was stabilized by a bite bar and two ear bars. The rectal temperature was monitored throughout the experiment and maintained at ~37 °C using warm air, and the respiration rate was monitored using a respiratory pillow sensor. Although FUS can penetrate through the intact mice skull, we performed the same surgical procedure as described in the 2PM study to add the glass window in the mouse skull to better mimic the experimental condition of the 2PM study. For each mouse, 6 FUS stimuli were applied to the same brain location with the same acoustic pressure and duty cycles as in the 2PM study.

Behavior test assay.

We used adeno-associated viruses (AAVs) to target the TRPV1 specifically to CaMKII-expressing neurons in the striatum of wild-type mice (C57BL/6, female, 6–8 weeks old) and determined whether sonothermogenetics could achieve causal control of the locomotor behavior by activating the basal ganglia circuit in freely moving mice. We selected the striatum as the targeted brain site to demonstrate the unique advantage of sonothermogenetic in facilitating noninvasive deep brain neuromodulation. $TRPV1^+$ mice were injected with 1.2 μL AAV5-CaMKII-TRPV1-p2A-DsRed (5.3×10^{12} vg/ml) at the left striatum (−3.0 mm dorsoventral, 0.0 mm anterior-posterior, and −2.3 mm mediolateral). Mice in the control group ($TRPV1^-$ mice) were injected with 0.5 μL of AAV5-CaMKII-DsRed (1.2×10^{13} vg/ml) to achieve the same viral vector dose. A miniaturized wearable transducer was custom-made using a lead zirconate titanate (PZT) ceramic resonator (DL-43, DeL Piezo Specialties, FL) with a frequency of 1.5 MHz, an aperture of 10 mm, and a radius of curvature of 10 mm. The PZT transducer with air backing was packaged in a 3D printed cone-shape housing (Fig. 5b). The 3D-printed housing was designed to fit a base plate that

was glued on the mouse skull 3 weeks post virus injection. The center point of the base plate was aligned with the striatum. Before the behavior testing, degassed ultrasound gel was filled in the cone, and the wearable transducer was plugged into the base plate. Following a 2-day adaption (1 hour per day) to the behavior test environment, the locomotor behavior of the mice in response to FUS stimulation was assessed. FUS sonication was repeatedly applied in both $TRPV1^+$ and $TRPV1^-$ mice using the similar acoustic parameters as those used in the 2PM study (frequency = 1.5 MHz, peak negative pressure = 1.3 MPa, duty cycle = 40%, PRF = 10 Hz, duration = 15 s). To reveal the parameter dependency of the behavior response, we evaluated another two FUS intensities in additional groups of $TRPV1^+$ and $TRPV1^-$ mice: peak negative pressure = 0, and 0.9 MPa. 0.9 MPa acoustic pressure was corresponding to approximately half of the acoustic intensity of 1.3 MPa. A total of 10 $TRPV1^+$ mice were sonicated at 1.3 MPa with n = 8 for all other groups. Each mouse was subjected to 3 or 5 repeated sonication. Previous studies showed that optogenetic stimulation at the same striatum location evoked rotational behavior in mice in the contralateral direction to the stimulation site [39]. We recorded the locomotor behavior of mice using a camera before, during, and after FUS sonication. The mean rotating angular speed and rotation direction were calculated and compared between $TRPV1^+$ and $TRPV1^-$ mice. The onset of rotation was defined as when the angular speed was > (mean + 3 × SD) of the angular speed obtained within a 5-s window before FUS on. The latency to rotation was calculated as the time delay between the starting time point of FUS sonication to the onset of animal rotation. An additional control experiment was performed with AAVs encoding TRPV1 injected in the left striatum, and the FUS sonication applied in the right striatum with the same FUS. A total of 4 mice were tested with each received 5 repeated sonication. The locomotor behavior of the mice was recorded and analyzed using the same method.

Histological analysis.

One practical consideration of thermal-based neuromodulation tools is the risk of damaging effects from the temperature increase. Two groups of mice without the injection of viral vectors were used to evaluate the safety of FUS exposure (n = 4 for each group). One group was sacrificed after FUS sonication with identical parameters to those used in the above study at 1.3 MPa. The other group served as the control without FUS exposure. Inspection of neuronal integrity, inflammation, and apoptosis by immunohistochemical staining of neurons (NeuN), astrocytes (GFAP), and microglia (Iba1) and staining for cell death (caspase-3 and TUNEL). The percentage of positive-stained cells over total DAPI-stained cells was calculated for each mice.

Statistics.

Data were analyzed using either a two-tailed t-test with unequal variance or ANOVA with the Bonferroni post hoc test. Statistical differences were considered significant whenever $P < 0.05$. All the graphs presented the results as average ± standard error of the mean (SEM).

Results

TRPV1 is a sonothermogenetic actuator.

High-amplitude Ca^{2+} influx was detected in the FUS-sonicated TRPV1-expressing cells ($TRPV1^{+}$) using fluorescence imaging (Fig. 1a, 1c). The maximum increase in fluorescence intensity (ΔF/F) was 0.46 on average (Fig. 1e). The TRPV1 antagonist capsazepine dramatically reduced Ca^{2+} influx in response to FUS stimulation in $TRPV1^{+}$ cells, suggesting that the observed Ca^{2+} influx was due to TRPV1 activation (Fig. S4). To determine whether FUS stimulation affected cells not expressing TRPV1, we stimulated cells that did not express TRPV1 ($TRPV1^{-}$) and these cells did not evoke significant Ca^{2+} influx (Fig. 1c, 1d). In both $TRPV1^{-}$ and $TRPV1^{+}$ cells, there were no significant changes in intracellular Ca^{2+} concentration without FUS stimulation. FUS stimulation had no detectable effects on cell viability (Fig. S5). These findings suggest that TRPV1 is an ultrasound-sensitive ion channel and can serve as a sonothermogenetic actuator.

Since FUS generates both thermal and mechanical effects, we then tested the hypothesis that FUS-induced thermal effect was sufficient to activate $TRPV1^{+}$ cells by performing an experiment to heat $TRPV1^{+}$ cells using water bath heating. We controlled the heating duration to increase the temperature to 42.2 ± 0.5 °C, which was approximately the same level as FUS-induced heating. We found that water-bath heating (Fig. 1b) had a similar success rate (Fig. 1d) and mean fluorescence intensity compared with those from FUS stimulation (Fig. 1f). This finding suggested that the FUS-induced thermal effect was sufficient to activate TRPV1-expressing cells *in vitro,* although the contribution of the ultrasound mechanical effect cannot be ruled out.

Sonothermogenetics selectively activates $TRPV1^{+}$ neurons in the mouse brain.

The custom-designed system for simultaneous FUS stimulation and 2PM imaging is shown in Fig. 2a. The full-width-half-maximum dimension of the FUS beam was 0.66 mm in the transverse plane and 5.8 mm in the coronal plane (Fig. 2b).

We observed that $TRPV1^{+}$ neurons switched from the silent to active state in response to FUS stimulation, while nearby neurons without TRPV1 overexpression were not affected (Fig. 2c). We consistently observed FUS activation of $TRPV1^{+}$ neurons, which showed strong Ca^{2+} influx (Fig. 2d and Fig. S6) and a high success rate of 75.0 ± 6.8% (Fig. 2e). FUS failed to activate the neurons in mice without TRPV1 overexpression ($TRPV1^{-}$), as seen from the minimal Ca^{2+} influx (Fig. 2d, lower panel) and a low success rate of 9.2 ± 3.8% (Fig. 2e), which was not significantly different from the control without FUS stimulation (Fig. 2d, 2e). These findings demonstrated the ability of sonothermogenetics to manipulate the activity of genetically selected neurons in the mammalian brain via TRPV1.

Temporally precise modulation of neural activity by sonothermogenetics.

Precise control of neural activity via sonothermogenetics depends on well-defined spatial and temporal control of ultrasound energy. The spatial precision of ultrasound energy delivery is achieved by the design of the FUS transducer (Fig. 2b). Here, we show temporally precise neuromodulation by sonothermogenetics (Fig. 3).

We found that reducing the PW duration to 7 s did not robustly evoke Ca^{2+} influx, but CW with 7 and 4 s durations repeatedly activated $TRPV1^+$ neurons in the mouse brain in a temporally precise fashion (Fig. 3a). Further decreasing the CW duration to 1 s did not consistently induce neuron activation. The success rate of 7-s CW (88.0 ± 7.3%) was significantly higher than that of 7-s PW stimulation (34.0 ± 5.1%) (Fig. 3b). The onset latencies and the relaxation times were quantified based on the successful activations from the efficacious FUS parameter sets, including 7-s PW, 7-s CW, and 4-s CW. The onset latencies were 3.3 ± 0.3 s and 2.5 ± 0.3 s for the 7-s CW and 4-s CW stimulation, respectively (Fig. 3c). The onset latency of the 4-s CW was significantly shorter than the latency for the 7-s PW (4.7 ± 0.5 s). In contrast to the onset time, CW did not reduce the relaxation time compared to PW. The normalized fluorescence intensity (ΔF/F) returned to half of its peak intensity within 14.6 ± 1.0 s and 14.9 ± 2.5 s for the 7-s CW and PW stimulation, respectively (Fig. 3d). These results demonstrated that sonothermogenetics is capable of controlling neural activities with high temporal precision.

FUS-induced local heating controls the success rate of sonothermogenetics.

The MR thermometry images recorded by the MR-guided FUS system (Fig. 4a) showed localized heating at the FUS-targeted brain location (Fig. 4b). The temperature curves verified that CW FUS raised the temperature faster than PW FUS (Fig. 4c), which explained the shortened onset latencies associated with 7-s CW and 4-s CW compared with 7-s PW (Fig. 3c). We quantified the average temperature change within the optical window of 2PM and found that the success rate of $TRPV1^+$ neuron activation was linearly correlated with the peak average temperature ($R^2 = 0.745$, Fig. 4d). This linear correlation between temperature and success rate further supports our hypothesis that FUS-induced heating is the dominant mechanism of TRPV1-mediated sonothermogenetics. It also suggests that the success rate of sonothermogenetics can be precisely controlled by FUS-inducing heating.

Sonothermogenetics evokes locomotor behavior.

Overexpression of TRPV1 in the left striatum was confirmed by immunohistochemistry staining of *ex vivo* brain slices using an anti-TRPV1 antibody (Fig. 5a). The developed miniaturized wearable FUS transducer for FUS sonication of freely moving mice is shown in Fig. 5b. FUS stimulation using the same acoustic pressure as those used in the study reported in Fig. 2 reversibly and repeatedly evoked rotational behavior in $TRPV1^+$ mice (Fig. 5c, 5d, and Movie S1). The rotational behavior was consistent with previous optogenetic [39], chemogenetic [42], and magnetothermal genetic [43] neuromodulation targeting the same brain location. In contrast, FUS failed to induce behavioral changes in the $TRPV1^-$ control mice (Fig. 5c, 5d, and Movie S2), indicating that the evoked behavior is due to the overexpressed TRPV1 that activated neurons in the striatum by FUS. The $TRPV1^+$ mice consistently turned contralateral to the sonication site in a total of 33 out of 38 trials (Fig. 5e, 1.3 MPa), which demonstrated causal control of animal behavior in a robust and repeatable fashion. In comparison, there was no significant change of the angular speed in the $TRPV1^-$ mice during FUS sonication. The average angular speed (2.24 ± 0.36 rev/min) of $TRPV1^+$ mice was approximately 7-fold higher than that (−0.33 ± 0.26 rev/min) of $TRPV1^-$ mice at 1.3 MPa stimulation (Fig. 5e). By reducing the FUS acoustic pressure to 0.9 MPa, the angular speed of $TRPV1^+$ mice remained significantly higher than that of the

control (0 MPa), but the average speed decreased to 0.79 ± 0.42 rev/min, suggesting that the animal behavior response can be tuned by the FUS parameters. FUS sonication at a different brain region contralateral to the virus injection site did not evoke significant changes in the animal's locomotion (Fig. 5e). This finding further validated that sonothermogenetics is spatially specific. $TRPV1^+$ mice responded rapidly to the sonothermogenetic stimulation with an onset latency of a few seconds (Fig. 5f), which was at a similar scale as the latency of Ca^{2+} response reported in Fig. 3c.

Sonothermogenetics is safe at the cellular level.

Cell nuclei are intact, and the neuron morphology is normal with FUS sonication compared with the control (Fig. 6a). No significant changes in the percentage of neurons, astrocytes, microglia, or apoptotic cells were found between the FUS^+ and FUS^- groups (Fig. 6b). TRPV1 overexpression by the viral vector also did not cause any significant changes in the percentages of neurons, astrocytes, microglia, and apoptotic cells (Fig. S7).

Discussion

Here, we describe a FUS technique for engaging and controlling activities of genetically selected neurons. This approach, we term "sonothermogenetics", is capable of noninvasive and temporally precise control over specific cell types in the deep brain, which cannot be achieved with existing neuromodulation techniques. This is the first study that provided direct evidence to show cell-type-specific activation of neurons *in vivo* in the mammalian brain by combining ultrasound and genetics. We also demonstrate for the first time that ultrasound combined with genetics can robustly control the behavior of freely moving mice by stimulating a deep brain target.

Most endogenous heat-sensitive ion channels, including TRPV1, are expressed in the hypothalamus and the peripheral nervous system, such as the dorsal root ganglia and trigeminal nodose ganglia [44-47]. There is also evidence that TRPV1 is expressed in other brain regions [45]. However, previous magnetothermal genetic neuromodulation studies have found that robust neuromodulation by activating TRPV1 requires sustained overexpression of TRPV1 in targeted neurons [43,48]. Indeed, we confirmed that the TRPV1 expression level was much higher in the virus-injected site than all other brain regions. Moreover, we did not observe FUS-induced activation of neurons or modulation of behavior in mice without TRPV1 overexpression, indicating that endogenous thermosensitive ion channels, even if they exist, are not sufficient for neural activation by FUS. While in the hypothalamus and peripheral nervous system, we may be able to take advantage of the endogenous TRPV1 to control neural activities if the expression level is sufficient, which warrants further research.

The direct effect of heating has been reported to elicit an inhibitory effect on neurons [49]. We investigated the potential confounding effect of FUS-induced heating by performing experiments in mice without TRPV1 overexpression ($TRPV1^-$). We found that heat generated by FUS was not adequate for activating naive neurons in the cortex of these mice ($TRPV1^-$ in Fig. 2d and 2e). Our behavior test in freely behaving mice further confirmed that the FUS energy used in the present study is insufficient to evoke either the excitatory

or inhibitory effect in TRPV1^{-} mice (Fig. 5). The unique advantage of sonothermogenetics in increasing a specific type of neuron's sensitivity to ultrasound allows selective control of these neurons, which clearly distinguishes sonothermogenetics from existing direct FUS neuromodulation (without genetics).

Optogenetics and chemogenetics are two of the most widely used genetic neuromodulation approaches. Chemogenetics suffers from poor spatial and temporal resolution, although it is capable of modulating neural activity noninvasively. In contrast, optogenetics has high spatiotemporal precision but often requires surgical implantation of optical fibers. The recent development of ultra-sensitive opsins enables noninvasive optogenetic neuromodulation by transcranial light illumination [6,7]; however, it loses the capability to spatially target the light at a selected brain site due to the diffusion of light. FUS has the capability to noninvasively target any depth of the mouse brain with high resolution. In addition to improved spatial targeting, sonothermogenetics can provide a temporal resolution at the scale of seconds, which is slower than optogenetics but much faster than chemogenetics. Recently, nanoparticle-mediated genetic neuromodulation approaches have been proposed for noninvasive control of neural activity, such as magnetothermogenetics [27,43] and upconversion nanoparticle-mediated optogenetics [50]. Different from these approaches, sonothermogenetics is completely noninvasive without the need for nanoparticle injection.

There are several limitations of the present study that warrant future research to better characterize sonothermogenetics. First, the 2PM calcium imaging used in this study had the limitation that it was not sensitive enough to test the possible inhibitory effect of FUS. Future studies can use this approach in the sensory or visual cortex to evaluate whether ultrasound-induced heat alone negatively affects the strength of evoked potentials by external stimuli. Secondly, this study performed safety evaluations after one session of FUS stimulation. Future longitudinal studies are needed to examine whether repeated exposure to FUS parameters used in conjunction with TRVP1 activation leads to consistent behavioral responses without inducing any side effects at the structural and molecular levels. Lastly, same as all single-element FUS transducers, the transducers used in this study had limited spatial resolution in the axial direction, as shown by the elongated ellipsoidal beam shape. The transducer design can be optimized in the future to improve the spatial resolution of sonothermogenetics.

Conclusion

The present study introduced a noninvasive neural modulation technique that utilized the FUS-induced brief, non-noxious thermal effect to selectively activate neurons genetically modified to express sonothermogenetic actuator TRPV1 in both superficial and deep brain. Sonothermogenetics activated TRPV1-overexpressing neurons at FUS-targeted location and evoked specific behavior changes in freely moving mice. This noninvasive and cell-type-specific neuromodulation approach with the capability to target the deep brain has the promise to advance the study of the intact nervous system and uncover new ways to treat neurological disorders.

Supplementary Material

Refer to Web version on PubMed Central for supplementary material.

Acknowledgments

This work was supported by the National Institutes of Health (NIH) BRAIN Initiative (R01MH116981) and NIBIB (R01EB027223 and R01EB030102). This work was supported by the Hope Center Viral Vectors Core at Washington University School of Medicine. We thank Dr. Hunter Banks, Dr. Lu Zhao, and Ms. Lindsey Brier for the insightful discussions. We thank D. Mingjie Li from the Hope Center Viral Vectors Core at Washington University for preparing the lentiviral and AAV vectors. We appreciate the help of Dr. James D. Quirk in thermometry mapping using magnetic resonance imaging. We thank Dr. Meaghan Creed for helping with viral injection. We also thank Dr. Si Chen for helping with immunofluorescence staining of *in-vitro* cells.

References

[1]. Follett KA, Weaver FM, Stern M, Hur K, Harris CL, Luo P, et al. Pallidal versus subthalamic deep-brain stimulation for Parkinson's disease. N Engl J Med 2010;362:2077–91. 10.1056/NEJMoa0907083. [PubMed: 20519680]

[2]. Cook MJ, O'Brien TJ, Berkovic SF, Murphy M, Morokoff A, Fabinyi G, et al. Prediction of seizure likelihood with a long-term, implanted seizure advisory system in patients with drug-resistant epilepsy: A first-in-man study. Lancet Neurol 2013;12:563–71. 10.1016/S1474-4422(13)70075-9. [PubMed: 23642342]

[3]. Yoon K, Lee W, Lee JE, Xu L, Croce P, Foley L, et al. Effects of sonication parameters on transcranial focused ultrasound brain stimulation in an ovine model. PLoS One 2019;14:e0224311. 10.1371/journal.pone.0224311. [PubMed: 31648261]

[4]. King RL, Brown JR, Newsome WT, Pauly KB. Effective parameters for ultrasound-induced in vivo neurostimulation. Ultrasound Med Biol 2013;39:312–31. 10.1016/j.ultrasmedbio.2012.09.009. [PubMed: 23219040]

[5]. Da Silva JA, Tecuapetla F, Paixão V, Costa RM. Dopamine neuron activity before action initiation gates and invigorates future movements. Nature 2018;554:244–8. 10.1038/nature25457. [PubMed: 29420469]

[6]. Gong X, Mendoza-Halliday D, Ting JT, Kaiser T, Sun X, Bastos AM, et al. An ultra-sensitive step-function opsin for minimally invasive optogenetic stimulation in mice and macaques. Neuron 2020;107:38–51.e8. 10.1016/j.neuron.2020.03.032. [PubMed: 32353253]

[7]. Chen R, Gore F, Nguyen Q-A, Ramakrishnan C, Patel S, Kim SH, et al. Deep brain optogenetics without intracranial surgery. Nat Biotechnol 2020:1–4. 10.1038/s41587-020-0679-9. [PubMed: 31919444]

[8]. Legon W, Sato TF, Opitz A, Mueller J, Barbour A, Williams A, et al. Transcranial focused ultrasound modulates the activity of primary somatosensory cortex in humans. Nat Neurosci 2014;17:322–9. 10.1038/nn.3620. [PubMed: 24413698]

[9]. Tufail Y, Matyushov A, Baldwin N, Tauchmann ML, Georges J, Yoshihiro A, et al. Transcranial pulsed ultrasound stimulates intact brain circuits. Neuron 2010;66:681–94. 10.1016/j.neuron.2010.05.008. [PubMed: 20547127]

[10]. Legon W, Ai L, Bansal P, Mueller JK. Neuromodulation with single-element transcranial focused ultrasound in human thalamus. Hum Brain Mapp 2018;39:1995–2006. [PubMed: 29380485]

[11]. Blackmore J, Shrivastava S, Sallet J, Butler CR, Cleveland RO. Ultrasound neuromodulation: a review of results, mechanisms and safety. Ultrasound Med Biol 2019;45:1509–36. 10.1016/j.ultrasmedbio.2018.12.015. [PubMed: 31109842]

[12]. Yoo SS, Bystritsky A, Lee JH, Zhang Y, Fischer K, Min BK, et al. Focused ultrasound modulates region-specific brain activity. Neuroimage 2011;56:1267–75. 10.1016/j.neuroimage.2011.02.058. [PubMed: 21354315]

[13]. Kubanek J, Shi J, Marsh J, Chen D, Deng C, Cui J. Ultrasound modulates ion channel currents. Sci Rep 2016;6:1–14. 10.1038/srep24170. [PubMed: 28442746]

[14]. Ye J, Tang S, Meng L, Li X, Wen X, Chen S, et al. Ultrasonic control of neural activity through activation of the mechanosensitive channel MscL. Nano Lett 2018;18:4148–55. [PubMed: 29916253]

[15]. Qiu Z, Guo J, Kala S, Zhu J, Xian Q, Qiu W, et al. The mechanosensitive ion channel piezo1 significantly mediates in vitro ultrasonic stimulation of neurons. iScience 2019;21:448–57. 10.1016/j.isci.2019.10.037. [PubMed: 31707258]

[16]. Oh S-J, Lee JM, Kim H-B, Lee J, Han S, Bae JY, et al. Ultrasonic neuromodulation via astrocytic TRPA1. Curr Biol 2019;29:3386–3401.e8. 10.1016/j.cub.2019.08.021. [PubMed: 31588000]

[17]. Qiu Z, Kala S, Guo J, Xian Q, Zhu J, Zhu T, et al. Targeted neurostimulation in mouse brains with noninvasive ultrasound. Cell Rep 2020;32:108033. 10.1016/j.celrep.2020.108033. [PubMed: 32814040]

[18]. Huang Y-S, Fan C-H, Hsu N, Wu C-Y, Chang C-Y, Hong S-R, et al. Sonogenetic modulation of cellular activities using an engineered auditory-sensing protein. Nano Lett 2020;20:1089–100. 10.1101/625533. [PubMed: 31884787]

[19]. Rabut C, Yoo S, Hurt RC, Jin Z, Li H, Guo H, et al. Ultrasound technologies for imaging and modulating neural activity. Neuron 2020;108:93–110. 10.1016/j.neuron.2020.09.003. [PubMed: 33058769]

[20]. Elias WJ, Lipsman N, Ondo WG, Ghanouni P, Kim YG, Lee W, et al. A randomized trial of focused ultrasound thalamotomy for essential tremor. N Engl J Med 2016;375:730–9. 10.1056/NEJMoa1600159. [PubMed: 27557301]

[21]. Martínez-Fernández R, Rodríguez-Rojas R, del Álamo M, Hernández-Fernández F, Pineda-Pardo JA, Dileone M, et al. Focused ultrasound subthalamotomy in patients with asymmetric Parkinson's disease: a pilot study. Lancet Neurol 2018;17:54–63. 10.1016/S1474-4422(17)30403-9. [PubMed: 29203153]

[22]. Leinenga G, Langton C, Nisbet R, Götz J. Ultrasound treatment of neurological diseases-current and emerging applications. Nat Rev Neurol 2016;12:161–74. 10.1038/nrneurol.2016.13. [PubMed: 26891768]

[23]. Zhu L, Altman MB, Laszlo A, Straube W, Zoberi I, Hallahan DE, et al. Ultrasound hyperthermia technology for radiosensitization. Ultrasound Med Biol 2019;45:1025–43. 10.1016/j.ultrasmedbio.2018.12.007. [PubMed: 30773377]

[24]. Bernstein JG, Garrity PA, Boyden ES. Optogenetics and thermogenetics: Technologies for controlling the activity of targeted cells within intact neural circuits. Curr Opin Neurobiol 2012;22:61–71. 10.1016/j.conb.2011.10.023. [PubMed: 22119320]

[25]. Dhaka A, Viswanath V, Patapoutian A. TRP ion channels and temperature sensation. Annu Rev Neurosci 2006;29:135–61. 10.1146/annurev.neuro.29.051605.112958. [PubMed: 16776582]

[26]. Huang H, Delikanli S, Zeng H, Ferkey DM, Pralle A. Remote control of ion channels and neurons through magnetic-field heating of nanoparticles. Nat Nanotechnol 2010;5:602–6. 10.1038/nnano.2010.125. [PubMed: 20581833]

[27]. Chen R, Romero G, Christiansen MG, Mohr A, Anikeeva P. Wireless magnetothermal deep brain stimulation. Science 2015;347:1477–80. 10.1126/science.1261821. [PubMed: 25765068]

[28]. Kim JH, Lee S-R, Li L-H, Park H-J, Park J-H, Lee KY, et al. High cleavage efficiency of a 2A peptide derived from porcine teschovirus-1 in human cell lines, zebrafish and mice. PLoS One 2011;6:e18556. 10.1371/journal.pone.0018556. [PubMed: 21602908]

[29]. Förster D, Dal Maschio M, Laurell E, Baier H. An optogenetic toolbox for unbiased discovery of functionally connected cells in neural circuits. Nat Commun 2017;8:1–12. 10.1038/s41467-017-00160-z. [PubMed: 28232747]

[30]. Holtmaat A, Bonhoeffer T, Chow DK, Chuckowree J, De Paola V, Hofer SB, et al. Long-term, high-resolution imaging in the mouse neocortex through a chronic cranial window. Nat Protoc 2009;4:1128–44. 10.1038/nprot.2009.89. [PubMed: 19617885]

[31]. Zinselmeyer BH, Dempster J, Wokosin DL, Cannon JJ, Pless R, Parker I, et al. Two-photon microscopy and multidimensional analysis of cell dynamics. Methods Enzymol 2009;461:349–78. 10.1016/S0076-6879(09)05416-0. [PubMed: 19480927]

[32]. Sato T, Shapiro MG, Tsao DY. Ultrasonic neuromodulation causes widespread cortical activation via an indirect auditory mechanism. Neuron 2018;98:1031–41. 10.1016/j.neuron.2018.05.009. [PubMed: 29804920]

[33]. Reynolds RP, Kinard WL, Degraff JJ, Leverage N, Norton JN. Noise in a laboratory animal facility from the human and mouse perspectives. J Am Assoc Lab Anim Sci 2010;49:592–7. [PubMed: 20858361]

[34]. Mohammadjavadi M, Ye PP, Xia A, Brown J, Popelka G, Pauly KB. Elimination of peripheral auditory pathway activation does not affect motor responses from ultrasound neuromodulation. Brain Stimul 2019;12:901–10. 10.1016/j.brs.2019.03.005. [PubMed: 30880027]

[35]. Pnevmatikakis EA, Soudry D, Gao Y, Machado TA, Merel J, Pfau D, et al. Simultaneous denoising, deconvolution, and demixing of calcium imaging data. Neuron 2016;89:285–99. 10.1016/J.NEURON.2015.11.037. [PubMed: 26774160]

[36]. Chen IW, Ronzitti E, Lee BR, Daigle TL, Dalkara D, Zeng H, et al. In vivo submillisecond two-photon optogenetics with temporally focused patterned light. J Neurosci 2019;39:3484–97. 10.1523/JNEUROSCI.1785-18.2018. [PubMed: 30833505]

[37]. Zhu L, Partanen A, Talcott MR, Gach HM, Greco SC, Henke LE, et al. Feasibility and safety assessment of magnetic resonance-guided high-intensity focused ultrasound (MRgHIFU)-mediated mild hyperthermia in pelvic targets evaluated using an in vivo porcine model. Int J Hyperthermia 2019;36:1147–59. 10.1080/02656736.2019.1685684. [PubMed: 31752562]

[38]. V. V. N. Kothapalli S, Altman MB, Zhu L, Partanen A, Cheng G, Gach HM, et al. Evaluation and selection of anatomic sites for magnetic resonance imaging-guided mild hyperthermia therapy: a healthy volunteer study. Int J Hyperth 2018;34:1381–9. 10.1080/02656736.2017.1418536.

[39]. Kravitz AV, Freeze BS, Parker PRL, Kay K, Thwin MT, Deisseroth K, et al. Regulation of parkinsonian motor behaviours by optogenetic control of basal ganglia circuitry. Nature 2010;466:622–6. 10.1038/nature09159. [PubMed: 20613723]

[40]. El Kouhen R, Surowy CS, Bianchi BR, Neelands TR, McDonald HA, Niforatos W, et al. A-425619 [1-isoquinolin-5-yl-3-(4-trifluoromethyl-benzyl)-urea], a novel and selective transient receptor potential type V1 receptor antagonist, blocks channel activation by vanilloids, heat, and acid. J Pharmacol Exp Ther 2005;314:400–9. 10.1124/jpet.105.084103. [PubMed: 15837819]

[41]. Lotteau S, Ducreux S, Romestaing C, Legrand C, Van Coppenolle F. Characterization of functional TRPV1 channels in the sarcoplasmic reticulum of mouse skeletal muscle. PLoS One 2013;8:58673. 10.1371/journal.pone.0058673.

[42]. Arenkiel BR, Klein ME, Davison IG, Katz LC, Ehlers MD. Genetic control of neuronal activity in mice conditionally expressing TRPV1. Nat Methods 2008;5:299–302. 10.1038/nmeth.1190. [PubMed: 18327266]

[43]. Munshi R, Qadri SM, Zhang Q, Rubio IC, del Pino P, Pralle A. Magnetothermal genetic deep brain stimulation of motor behaviors in awake, freely moving mice. Elife 2017;6:1–26. 10.7554/eLife.27069.

[44]. Güler AD, Rainwater A, Parker JG, Jones GL, Argilli E, Arenkiel BR, et al. Transient activation of specific neurons in mice by selective expression of the capsaicin receptor. Nat Commun 2012;3:1–10. 10.1038/ncomms1749.

[45]. Roet M, Jansen A, Hoogland G, Temel Y, Jahanshahi A. Endogenous TRPV1 expression in the human cingulate- and medial frontal gyrus. Brain Res Bull 2019;152:184–90. 10.1016/j.brainresbull.2019.07.018. [PubMed: 31325598]

[46]. Lamas JA, Rueda-Ruzafa L, Herrera-Pérez S. Ion channels and thermosensitivity: TRP, TREK, or both? Int J Mol Sci 2019;20:2371. 10.3390/ijms20102371.

[47]. Pecze L, Jósvay K, Blum W, Petrovics G, Vizler C, Oláh Z, et al. Activation of endogenous TRPV1 fails to induce overstimulation-based cytotoxicity in breast and prostate cancer cells but not in pain-sensing neurons. Biochim Biophys Acta - Mol Cell Res 2016;1863:2054–64. 10.1016/j.bbamcr.2016.05.007.

[48]. Stanley SA, Kelly L, Latcha KN, Schmidt SF, Yu X, Nectow AR, et al. Bidirectional electromagnetic control of the hypothalamus regulates feeding and metabolism. Nature 2016;531:647–50. 10.1038/nature17183. [PubMed: 27007848]

[49]. Owen SF, Liu MH, Kreitzer AC. Thermal constraints on in vivo optogenetic manipulations. Nat Neurosci 2019;22:1061–5. 10.1038/s41593-019-0422-3. [PubMed: 31209378]

[50]. Chen S, Weitemier AZ, Zeng X, He L, Wang X, Tao Y, et al. Near-infrared deep brain stimulation via upconversion nanoparticle–mediated optogenetics. Science (80−) 2018;359:679–84. 10.1126/science.aaq1144.

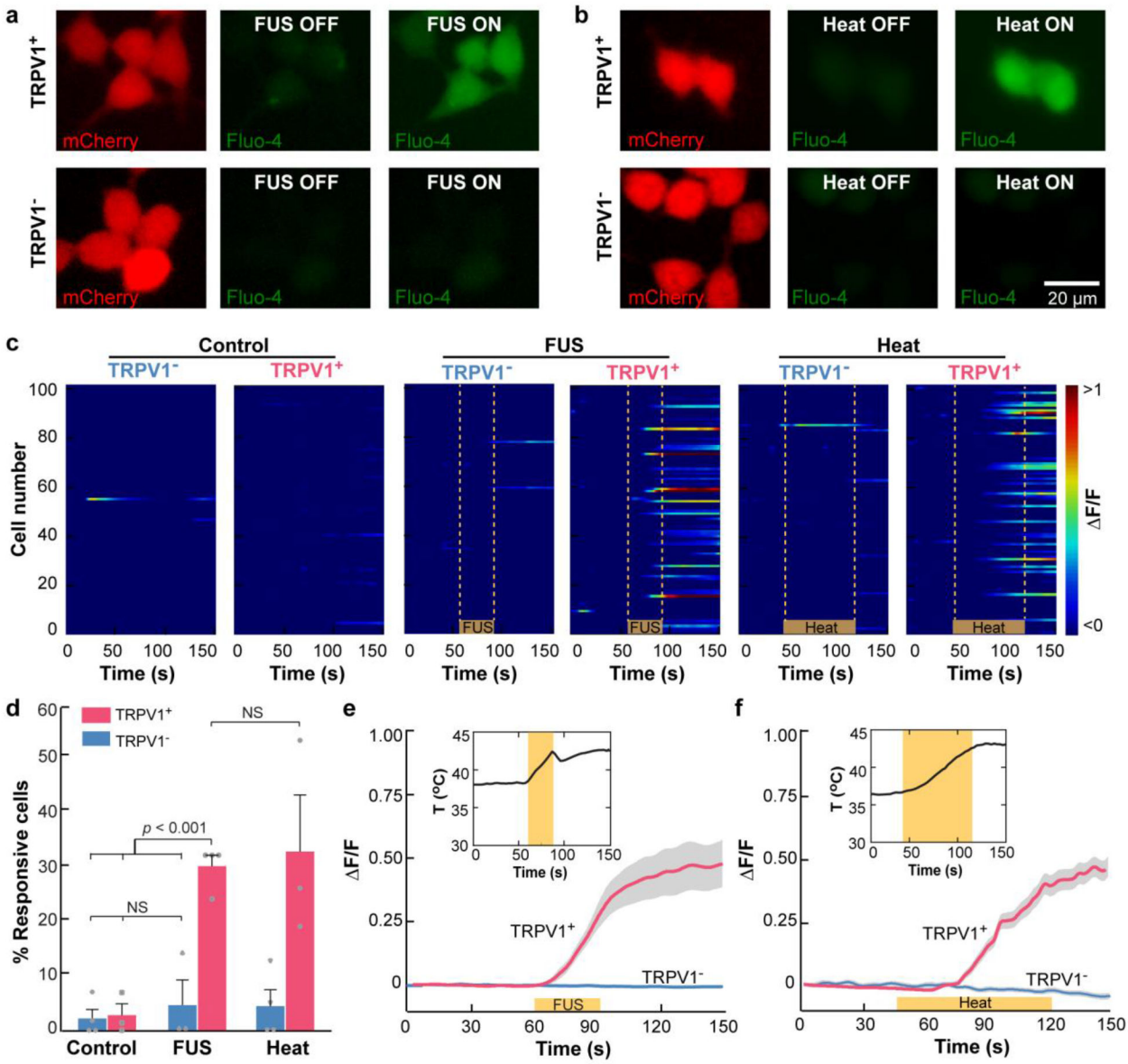

Fig. 1. TRPV1 enables FUS activation of HEK293T cells *in vitro*.

(**a, b**) Fluorescence images of HEK293T cells. Red: HEK293T cells expressing mCherry with the TRPV1 ion channel (TRPV1$^+$, top row) or without the TRPV1 ion channel (TRPV1$^-$, bottom row). Green: Intracellular Ca^{2+} before and after (**a**) FUS stimulation and (**b**) water-bath heating. (**c**) Heatmap of the normalized Ca^{2+} fluorescence intensity change (ΔF/F) of 100 randomly selected TRPV1$^+$ and TRPV1$^-$ cells from 3–4 independent trials in the control group without any stimulation (left panel), the FUS group (middle panel), and the heating group (right panel). The yellow lines indicate FUS on in the FUS group and heat on in the water-bath heating group. (**d**) Percentage of TRPV1$^+$ and TRPV1$^-$ cells within the FOV of the fluorescence microscope that responded to FUS stimulation and water-bath heating, respectively. Cells in the control group were not stimulated. The error bar indicates the standard error of the mean (SEM). Normalized fluorescence intensity change (ΔF/F) of TRPV1$^+$ and TRPV1$^-$ induced by (**e**) FUS stimulation and (**f**) water bath

heating. The solid lines indicate the mean, and shaded gray represents SEM. The insert shows the corresponding temperature curve.

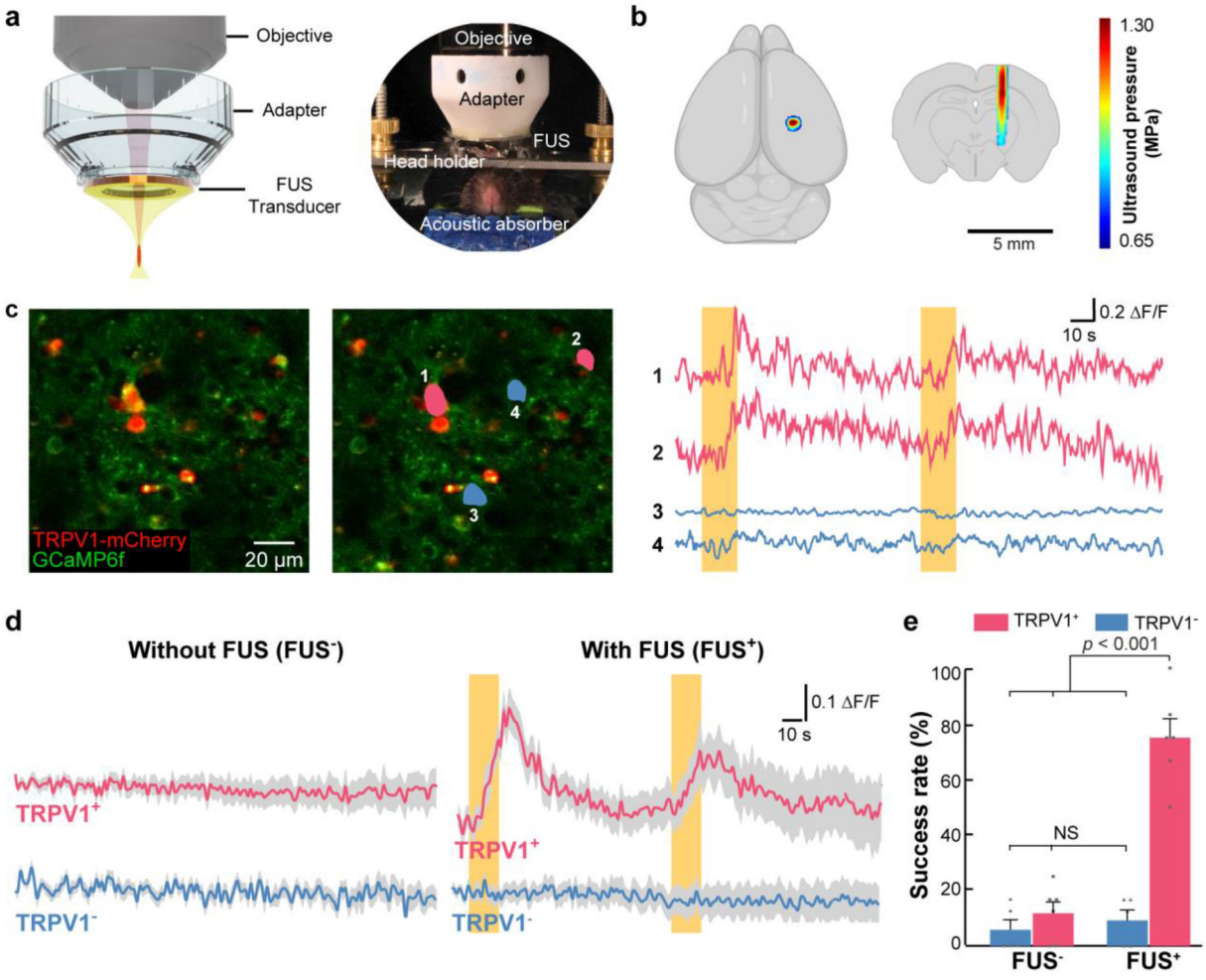

Fig. 2. Sonothermogenetics selectively activates TRPV1$^+$ neurons *in vivo*.

(a) Schematic illustration (left) and a photo (right) of the 2PM setup that couples a ring-shaped FUS transducer with the microscope objective using a customized adapter. The mouse head was fixed by a holder to minimize motion artifacts in 2PM imaging. An acoustic absorber was placed underneath the mouse head to decrease the reflection of the ultrasound pulses from the bottom of the mouse head. (**b**) The FUS pressure distribution maps in the transverse and coronal planes are superimposed on drawings of the mouse brain. (**c**) A representative 2PM image of the mouse cortex *in vivo* is shown on the left. The image on the right highlights two neurons (1 and 2 in pink) expressing both TRPV1-mCherry and GCaMP6f and two neurons (3 and 4 in blue) expressing only GCaMP6f without TRPV1. The Ca^{2+} fluorescence intensity changes over time of the 4 neurons are shown next to the 2PM image. (**d**) Average Ca^{2+} fluorescence intensity curves for mice with and without TRPV1 overexpression with FUS stimulation (FUS$^+$) and without FUS stimulation (FUS$^-$) (n = 17 neurons from 6 TRPV1$^+$ mice and n = 16 neurons from 5 TRPV1$^-$ mice). Solid lines and the shaded area indicate the mean and the SEM. Yellow bars indicate FUS on. **(e)** Comparison of the averaged success rate of these selected neurons with and without FUS stimulation. The error bar represents the SEM.

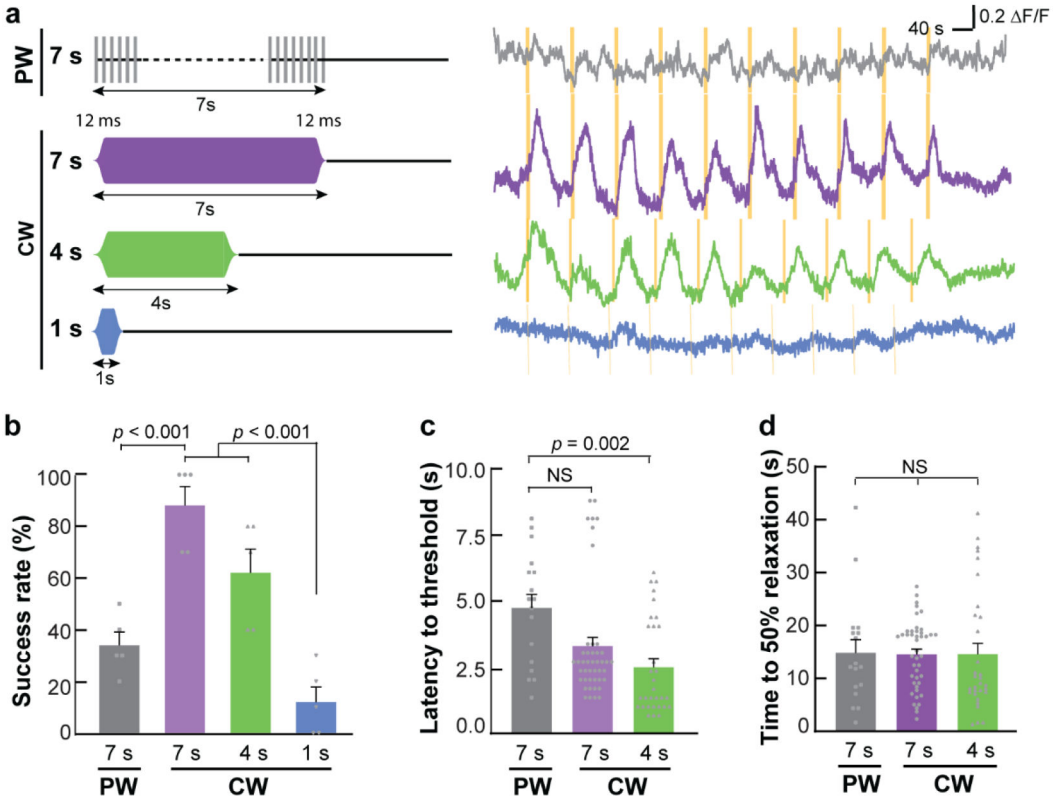

Fig. 3. Temporally precise modulation of neural activity by sonothermogenetics.

(**a**) Illustration of the smoothed pulsed wave (PW) and continuous wave (CW) (left). Representative Ca^{2+} dynamics in response to 10 repeated FUS stimulations using different parameters (right). Yellow bars indicate the FUS stimulation time. Quantification of (**b**) success rate, (**c**) latency, and (**d**) time to 50% relaxation for different FUS parameters (error bars indicate SEM).

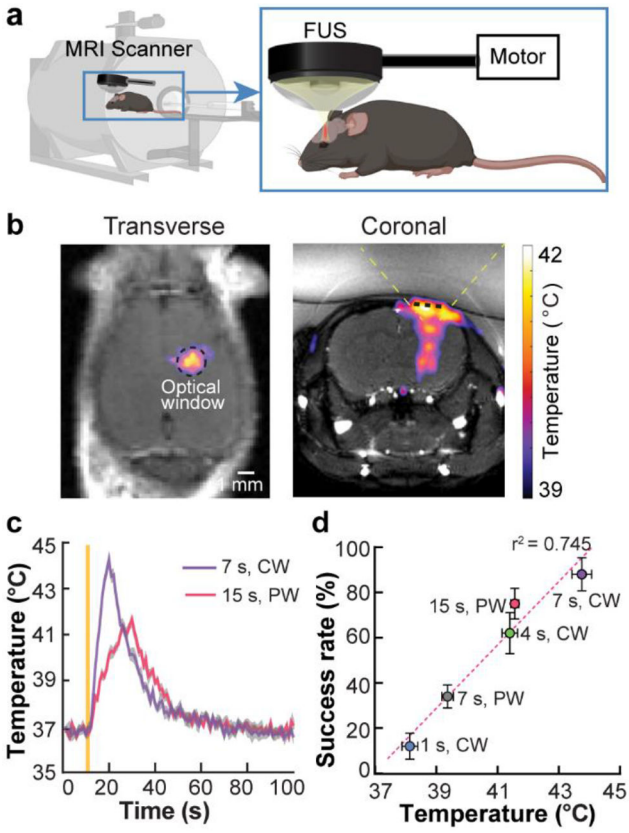

Fig. 4. Control of sonothermogenetics by FUS-induced local heating.

(a) Integration of FUS with MR for imaging FUS-induced temperature rise in the mouse brain by *in vivo* real-time MR thermometry. (**b**) Spatial distribution of FUS-induced heating in the transverse and coronal views as imaged by MR thermometry. The location of the optical window for 2PM is indicated by the black dashed circle in the transverse plane and by the black dashed line in the coronal plane. The yellow dashed lines in the coronal plane illustrate the FUS beam. (**c**) Mean temperature within the optical window as a function of time for both PW and CW stimulation. The solid yellow line indicates the onset of FUS sonication. (**d**) A linear correlation between the peak temperature associated with each FUS parameter and the success rate of $TRPV1^+$ neuron activation (Fig. 2e and 3b) was identified ($R^2 = 0.745$). Error bars indicate SEM.

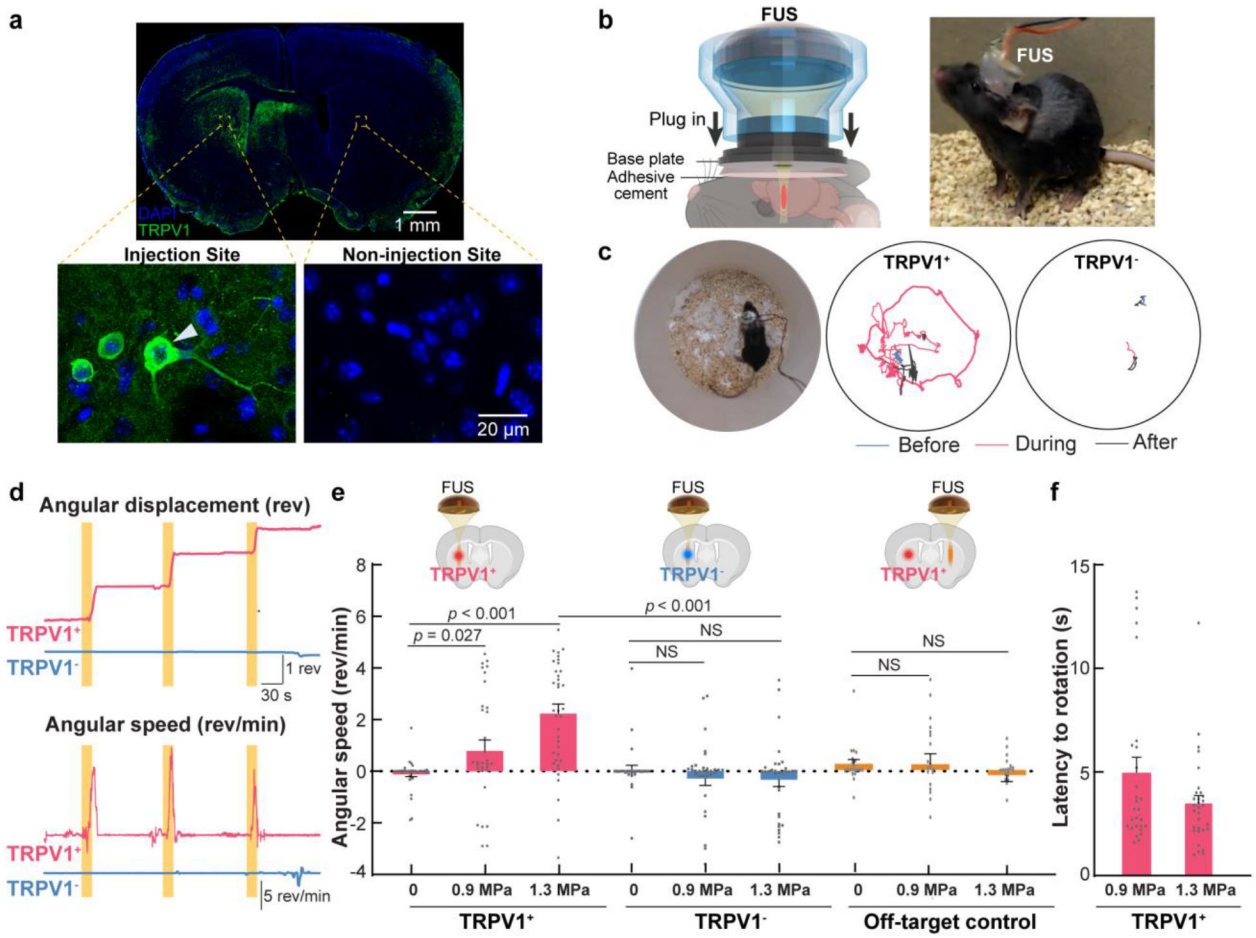

Fig. 5. Sonothermogenetic modulation of mouse locomotor behavior.

(**a**) Expression of TRPV1 in the mouse brain that was extracted one month after the viral injection and assessed by immunofluorescence staining with an anti-TRPV1 antibody. The arrowhead points at an example of TRPV1-positive neuron. **(b)** Experimental setup for *in vivo* sonothermogenetic stimulation of the striatum in freely moving mice. The miniaturized wearable FUS transducer was plugged into a base plate adhered on the mouse head. **(c)** Representative trajectories recorded in TRPV1^{+} and TRPV1^{-} mice before (blue), during (red), and after (gray) FUS stimulation (each stimulation was 15-s long and 1.3 MPa). **(d)** The angular displacement (top) and angular speed (bottom) of the TRPV1^{+} and TRPV1^{-} mice shown in (**c**). (Yellow bars indicate the three repeated FUS stimulations. **(e)** Comparison of the mean angular speed of TRPV1^{+} mice, TRPV1^{-} mice and off-target control mice with FUS stimulation at different acoustic pressure = 0, 0.9, and 1.3 MPa. TRPV1 expression and FUS sonication location for different groups are illustrated in the upper insert. The positive and negative values indicate rotation in the contralateral and ipsilateral directions, respectively. **(f)** The behavior onset latency of TRPV1^{+} mice in response to FUS stimulation. Error bars represent the standard error of the mean.

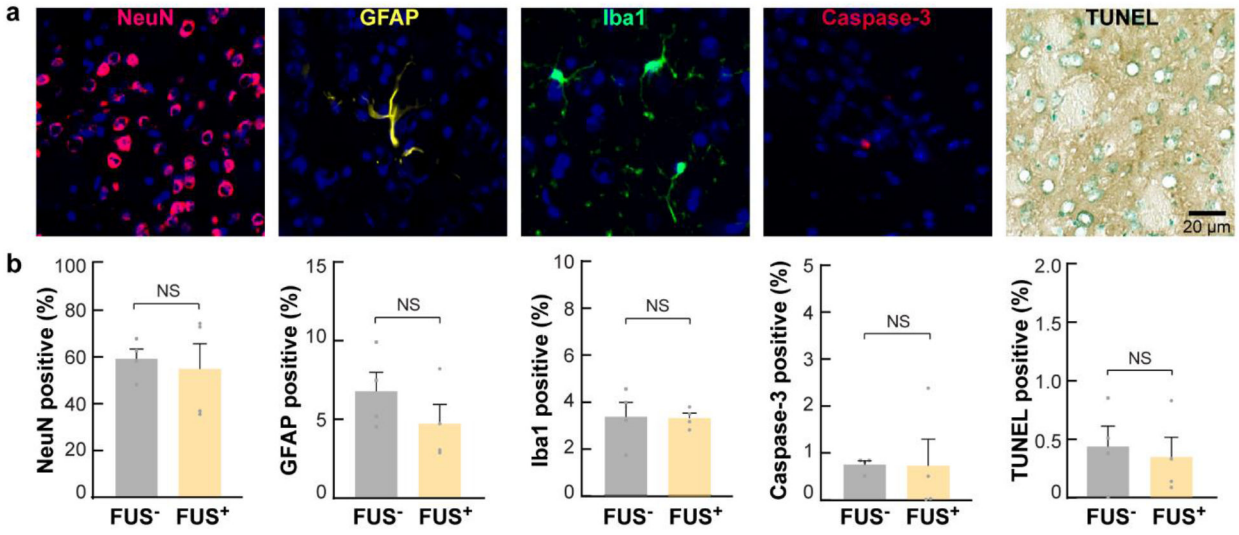

Fig. 6. Sonothermogenetics is safe at the cellular level.

(a) Evaluation of neuronal integrity, inflammation, and apoptosis after FUS exposure in the FUS-targeted brain location using immunohistochemical staining of neurons (NeuN), astrocytes (GFAP), microglia (iba1), caspase-3, and TUNEL. In the fluorescence images, blue indicates the DAPI-stained nuclei, and other pseudocolors indicate different cell types. (**b**) Percentages of positively stained cells to DAPI-stained cells within the FUS-targeted brain location in FUS-sonicated mice compared to those in mice without FUS sonication.